Redesigned Solid Rocket Motor Case-to-Nozzle Joint Development

Roger V. Cook,* Robert A. Morstadt,† Steven V. Hicken,‡ and Michael J. O'Malley§
Thiokol Corporation, Brigham City, Utah 84302

The case-to-nozzle joint in the Space Shuttle solid rocket motor is designed to provide thermal protection to the case and nozzle metal parts and to the O-ring seals during motor operation and subsequent heat soak. As a part of the redesign effort, several design improvements were incorporated into the joint configuration. These included an unvented bonded joint, the addition of a pressure-actuated flap gap next to the bondline, the addition of an adhesive wiping O-ring, and the addition of 100 bolts in the radial direction to restrict joint movement. With the new design features, it became necessary to develop a new nozzle installation procedure. Also, a number of hot-fire static tests were performed before the joint could be used in a flight motor. In several of these tests, flaws were deliberately placed in the case-to-nozzle bondline and O-rings to determine how the redesigned joint would function with a portion of the redundant sealing system disabled prior to motor operation. Each flaw condition tested was accompanied by a flow/thermal analysis. Once these analyses had been verified, analyses were then used to examine other flaw configurations that were not being tested.

Introduction

THE case-to-nozzle joint in the Space Shuttle solid rocket motor (SRM) is designed to provide thermal protection to the case and nozzle metal parts and to the O-ring seals during the motor operation and subsequent heat soak. Prior to flight space transportation system STS-51-L, the case-to-nozzle joint contained a putty joint filler shown in Fig. 1. As a part of the redesign effort the case-to-nozzle joint configuration was reviewed for improved safety and performance.

The case-to-nozzle joint in the redesigned solid rocket motor (RSRM), as shown in Fig. 1, was developed according to the criteria established in the contract end item (CEI) specification.[1] Major design improvements included replacing the putty-joint filler with an unvented bonded joint, the addition of a pressure-actuated flap gap next to the bondline, the addition of an adhesive-wiping O-ring, and the addition of 100 bolts in the radial direction to restrict joint movement. With the addition of the new design features, it became necessary to develop a new nozzle installation procedure. Also, a number of hot-fire static tests were performed before the joint could be used in a flight motor. In several of these tests, flaws were deliberately placed in the joint bondline and through O-rings to determine how the redesigned joint would function with a portion of the redundant sealing system disabled prior to motor operation. Each flaw condition tested was accompanied by a flow/thermal analysis. Once these analyses had been verified, other possible flaw configurations, that were not tested, were also analyzed.

Testing of the joint has demonstrated that the design is impervious to the conditions inside the motor chamber during the 2-min burn when temperature and pressure reach approximately 6000°F and 1000 psi. The joint is tolerant of flaws that may be introduced into the bondline or the O-rings during the assembly process. The performance of the joint has also been verified by the six successful STS flights at the time of this writing.

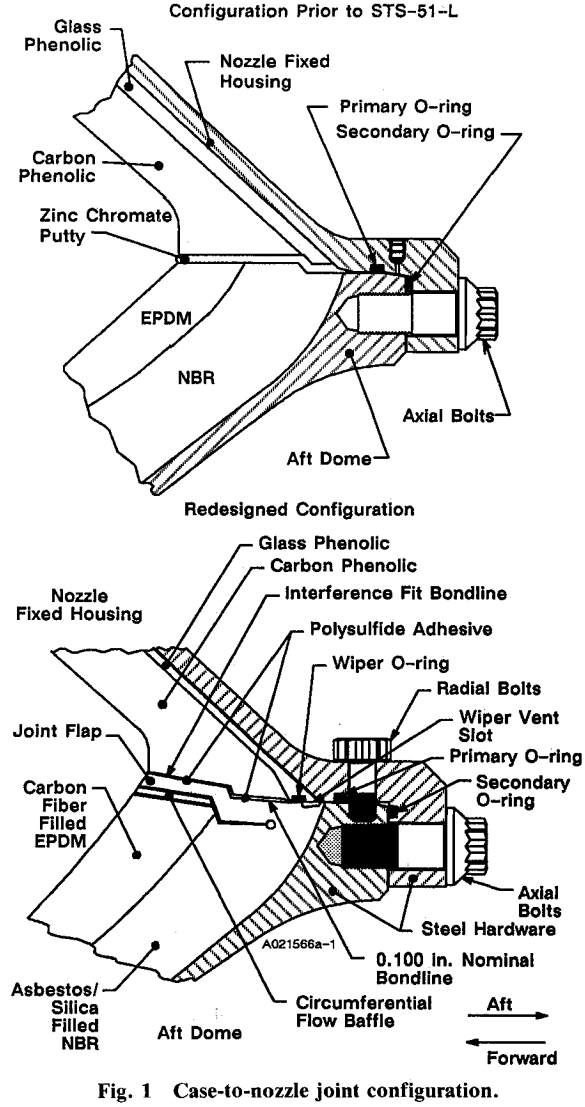

Fig. 1 Case-to-nozzle joint configuration.

Presented as Paper 89-2773 at the AIAA/ASME/ASEE/SAE 25th Joint Propulsion Conference, Monterey, CA, July 10-12, 1989; received Aug. 17, 1989; revision received Nov. 17, 1989.

*Design Engineer, Nonmetallic Component Design/Space Operations. Member AIAA.

†Scientist, Analysis Support/Space Operations. Member AIAA.

‡Senior Design Engineer, Nonmetallic Component Design/Space Operations.

§Senior Engineer, Analysis Support/Space Operations. Member AIAA.

Discussion

Prior to STS-51-L, the case-to-nozzle joint configuration consisted of the nozzle-fixed housing mated to the aft dome as shown in Fig. 1. A zinc-chromate putty was used as a filler in the gap in the two components. Two O-rings were located aft of the insulation to provide the pressure sealing capability of the joint. This joint functioned successfully on all flights in which it was employed; however, several design improvements were made during the redesign period. These improvements were concerned with reducing the probability of O-ring erosion. In past flights, chamber pressure had reached the O-rings through leak paths in the zinc chromate putty and by chamber pressure forcing the joint open during motor operation.

During the redesign period, the case-to-nozzle joint was reviewed for improved reliability. The redesign that followed was implemented in accordance with the following ground rules based on the CEI specification.

1) Internal insulation shall protect the metal parts and seals from damage.

2) The geometric design envelope must meet the following criteria: a) Joint insulation cannot extend radially in board of the nozzle boss metal surface more than 0.8 in. b) Maximum insulation thickness at the nozzle boss cannot increase significantly to retain sufficient clearance for casting. c) The maximum diameter of the fixed housing insulation must be smaller than the nozzle boss diameter.

3) Internal insulation shall be designed to meet a minimum thermal safety factor of 2 for 2 in. on each side of the aft dome-to-nozzle, fixed, housing insulation interface based on $M+3\sigma$ predicted material decomposition depth.

4) Internal insulation shall withstand slag accumulation.

5) Internal insulation shall accommodate joint deflection due to motor operation and temperature changes.

6) Internal insulation shall accommodate the effects of circumferential flow.

7) The case-to-nozzle joint shall be an unvented bonded joint.

8) The joint insulation configuration shall preclude a straight line path through the joint.

9) The insulation shall accommodate preflight demating without damage to the metal parts.

The following sections discuss, in detail, the various aspects of the case-to-nozzle joint redesign effort.

Design Features

The insulation materials that comprise the two sides of the joint are similar to those used in the pre-STS-51-L design. The aft-dome portion of the joint insulation as shown in Fig. 1 consists of a combination of carbon-fiber-filled ethylene propylene diene monomer (CF/EPDM) and asbestos silica-filled acrylonitrile butadiene rubber (NBR). The nozzle-fixed housing insulation consists of a carbon phenolic (CP) and glass phenolic combination. The configuration of the fixed housing insulation is made by machining the insulation surfaces, and the aft-dome insulation configuration is made by net molding the part. These two major components of the joint are bonded together during joint assembly. The nozzle-fixed housing contains three Viton O-rings. The forward O-ring is the wiper and is not intended to be a seal. It functions as a barrier to keep the adhesive from extruding aft and contaminating the adjacent (primary) O-ring during assembly. The two O-rings in the aft end of the joint (primary and secondary) provide the redundant pressure sealing ability of the joint.[2]

One of the major constraints in the design of this joint is the geometric design envelope. The propellant casting core is inserted through the aft end of the aft segment. The radius of this core is approximately 0.8 in. smaller than the radius of the aft-dome nozzle boss opening shown in Fig. 2. The nozzle must also be inserted through the aft end with the nozzle cowl outside diameter being approximately 1.3 in. on the radius smaller than the nozzle boss. For these reasons, it was determined that the joint insulation on the aft-dome side could not extend radially in board of the nozzle boss metal surface by more than 0.8 in. It was also determined that the maximum insulation thickness at the nozzle boss could not increase significantly since the clearance between the insulation and the inserted casting core creates an annulus through which all of the aft-segment propellant is cast as shown in Fig. 3. A reduction in this clearance would reduce the rate at which the motor is cast and may cause the minimum cast rate requirement to be violated.

The assembly mode of the case-to-nozzle joint (i.e., the sliding of the fixed housing into the aft-dome nozzle boss) also requires that the maximum diameter of the fixed-housing insulation be smaller than the nozzle-boss diameter. These constraints require the entire joint insulation configuration be designed within the 0.8-in. height and the existing maximum thickness envelope.

The joint insulation configuration is designed to provide a minimum thermal safety factor of 2 based on $M+3\sigma$ material decomposition depths (MDD). The critical area for the joint is defined to be 2 in. on each side of the mating joint insulation interface measured on surfaces which normally see erosion. Both the nozzle-fixed housing and the aft-dome joint insulation have been evaluated through testing and analysis and meet the 2.0 safety factor requirement at the joint.[3] In all cases, the remaining virgin thickness over metal parts is equal to or greater than 50% of the minimum thickness. Since the $M+3\sigma$ MDD numbers incorporate the effects of slag, the joint is designed to withstand slag accumulation.

A pressurization slot or flap gap was placed on the aft-dome side of the joint as shown in Fig. 4. This slot provides a stress relief mechanism, which enables the joint insulation to accommodate joint movement due to thermal effects during storage and motor pressurization following ignition. The CEI specification limits the propellant mean bulk temperature (PMBT) to between 40 and 90°F at launch. Preliminary structural analysis indicated that the slot entrance could open as much as 0.52 in. at motor ignition for a 40°F PMBT firing. In order to accommodate this deflection, the aft-dome insulation is designed with a joint stress relief flap. The joint flap is manufactured out of NBR rather than CF/EPDM due to its superior strain capabilities. An O-ring is included in the terminus of the flap gap to reduce the stress in the flap terminus as the joint deflects open.

The joint configuration is able to accommodate circumferential flow, which can occur at the case-to-nozzle joint as the nozzle is vectored. This is accomplished by adding a circumferential flow baffle in the joint stress relief flap gap. The baffle consists of NBR plies, which are alternately bonded to the joint stress relief flap and the CF/EPDM around the circumference. The baffle acts to redirect the flow into the flap gap and preclude significant circumferential flow velocities.

The spacing between the bonded regions of the circumferential flow baffle is specifically designed to allow up to 0.52-in. deflection without stressing the baffle or its bondlines. This allows the flap to remain in contact with the carbon phenolic insulation throughout joint geometry changes caused by temperature and motor pressure variations.

Joint Bonding

The redesigned case-to-nozzle joint incorporates the use of an adhesive to bond the adjoining insulation components together shown in Fig. 1. The function of the adhesive is to serve as a heat barrier for the metal hardware and to reduce the likelihood of hot gases reaching the primary and secondary O-rings. It is also intended to direct initial motor flow into the flap gap, which will place the joint bondline into compression during motor operation.

The joint is designed with a taper on the insulation surfaces to aid in the bonding operation. This results in a closing action between the two parts on assembly and is helpful in allowing air to bleed out of the bondline before the adhesive flow seals it in. The joint stress relief flap gap also contributes to the

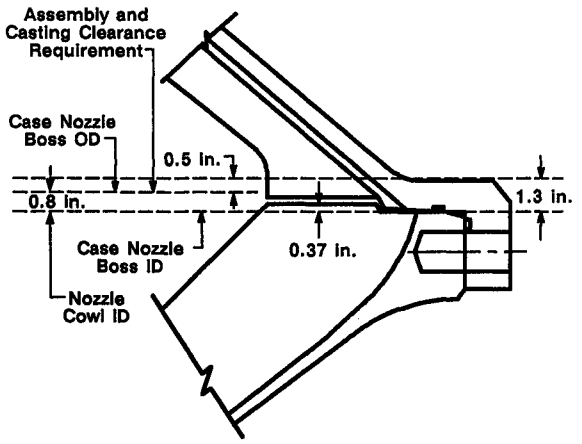

Fig. 2 Geometric design envelope.

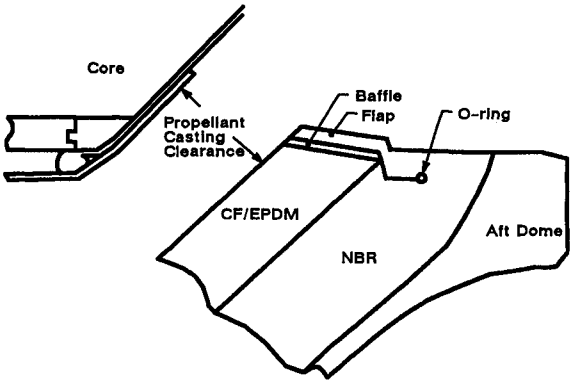

Fig. 3 Aft-dome propellant casting clearance.

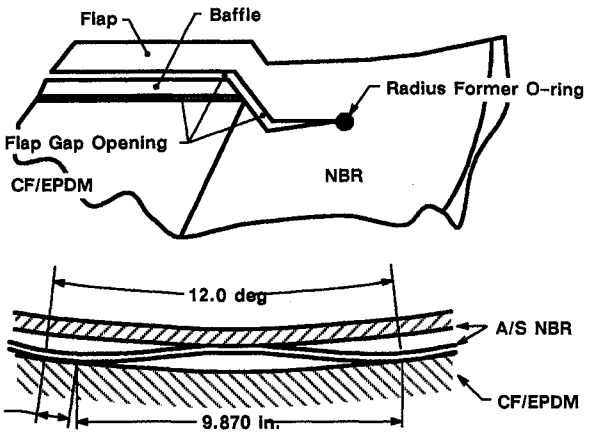

Fig. 4 Case-to-nozzle joint pressurization slot or flap gap with the circumferential flow baffle.

bond. It tends to be open in its natural unassembled state due to shrinkage of the rubber during cure shown in Fig. 4, which results in an engagement between the flap and the fixed housing phenolics during assembly. This, in turn, results in a thin bondline at the forward portion or entrance of the joint.

The joint bondline is designed as a step configuration, which precludes direct flow or radiation heating into the joint in the event of a bondline leak. The constraint to preclude the gas from having a straight line flow path into the joint is satisfied by having both the angled bondline into the joint and a step in the bondline shown in Fig. 1.

The adhesive used in the bonded joint would replace the zinc chromate putty-gap filler employed in the pre-STS-51-L, case-to-nozzle joint. Several candidate adhesives were selected for evaluation from the silicone room-temperature vulcanization (RTV), urethane, polysulfide, and epoxy-adhesive families. The criteria for selecting the baseline adhesive was based on the following case-to-nozzle joint design goals. 1) The bonded case-to-nozzle joint bondline shall not fail due to motor operation or thermal effects during storage; 2) the bondline shall accommodate preflight demating without damage to the NBR insulation or the baffle; 3) the bondline shall accommodate joint deflection due to motor operation and temperature changes; 4) the adhesive shall have a long potlife and shall be in a viscosity range that will facilitate the assembly.

The first two goals set a quantified band that the adhesive strength must fall within. The tensile and peel strengths must be high enough to restrict the bondline from failing during motor operation or thermal contraction during storage. The adhesive also had to be weaker than the baffle CF/EPDM interface or the NBR insulation in case a preflight nozzle disassembly became necessary. These two requirements would have been impossible to meet simultaneously if it were not for the addition of the flap gap to the design configuration.

The chamber pressure penetrates the flap gap during motor operation. The flap is held against the fixed-housing phenolics keeping the joint bondline in compression. This avoids the need for a high-strength adhesive since the only significant tensile loads are produced by thermal contraction during storage. Since the tensile loads applied to the bondline during storage are low, on the order of 35 psi at a PMBT of 40°F, the determining factor on the strength requirements became the force necessary to disassemble a case-to-nozzle joint preflight without damage.[4] Lower strength silicone RTVs and polysulfide adhesives were the only adhesives tested with maximum strengths weaker than the surrounding materials but also with high enough strengths to not fail during storage.

The third goal specifies that the adhesive has a minimum elongation of 20%. This strain level was determined analytically for a PMBT of 40°F.[4] Both the silicone RTV and the polysulfide adhesive selected for further testing have strain capabilities many factors greater than this.

Case-to-Nozzle Joint Assembly Process

The method of assembling the case-to-nozzle joint was developed through the nozzle joint assembly demonstration (NJAD).[5] In this test, different methods of applying the adhesive and mating the nozzle-fixed housing to the aft dome were evaluated in a series of practice assemblies using full-scale hardware. The finalized process involves applying the adhesive to the insulation surface of the aft dome while the segment is oriented with the aft end up. A screed is run over the surface to form the adhesive into a predefined profile. The nozzle with the nozzle-fixed housing is then lowered into the opening in the aft dome forcing the adhesive to fill into the entire bondline. The wiper O-ring located at the aft end of the bondline functions as a barrier to keep the adhesive from extruding aft and contaminating the primary O-ring during joint assembly. After the nozzle has been seated, the fixed housing is attached to the aft dome with 100 bolts in the axial direction. This provides the structural support in the joint. An additional 100 bolts are attached in the radial direction to restrict the joint from opening due to chamber pressure during motor operation.

The joint assembly process requires up to 2 h from the time that the adhesive is applied onto the aft dome until the nozzle-fixed housing is seated. During this time the adhesive must remain on a vertical surface in the shape formed by the screed without slumping. Therefore, the selected adhesive must be available in a thixotropic paste consistency. Also, in the final inches of the assembly, it is beneficial to have a lower viscosity to facilitate the adhesive flowing to all portions of the bondline. This requires that the adhesive setup slowly during

the first 2 h after mixing. Of the two adhesives still considered, the polysulfide was available in a thixotropic paste and in a greater range of working lives. This ease of application factor along with better flow characteristics demonstrated in NJAD resulted in the selection of the polysulfide adhesive as the baseline adhesive.

A recurring problem in the NJAD tests was air entrapment between the wiper O-ring and the adhesive during assembly. As the nozzle was lowered into place, the air pocket became pressurized and extruded in the direction of least resistance, through the bondline. This created a leak path directly to the wiper O-ring after the adhesive had cured. At the aft end of the leak path adjacent to the wiper O-ring, was a large circumferential void that would expose a significant portion of the wiper O-ring to hot gases if the joint were to be pressurized.

Minimizing the quantity of air entrapped during assembly and providing a path for the air that is entrapped to bleed out were the methods pursued to eliminate this problem. Modifications to the adhesive profile formed by the screed reduced the amount of air entrapped, but could not eliminate it completely. Grooves or slots were notched into the aft-dome NBR insulation to allow the remaining entrapped air to vent past the wiper O-ring during assembly shown in Fig. 5. These grooves were placed immediately aft of the final resting location of the wiper O-ring. By the time the nozzle is seated, the wiper O-ring has passed over the grooves, thus venting the air pocket, and has come to rest on the solid NBR surface.

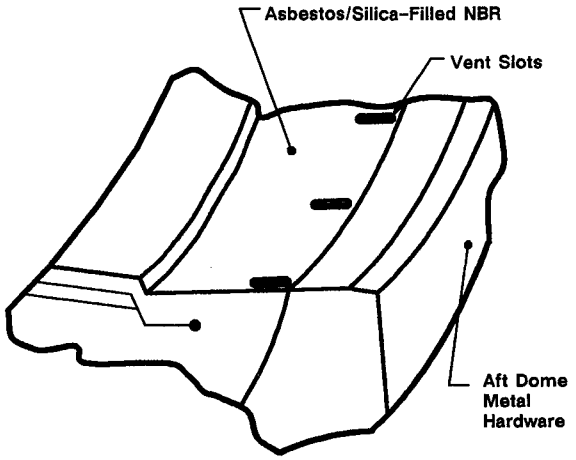

Fig. 5 Case-to-nozzle joint-wiper vent slots.

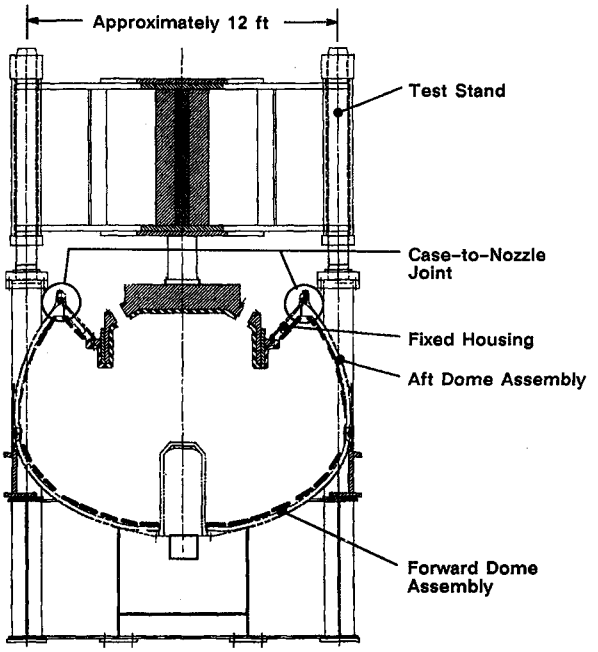

Fig. 6 Nozzle joint environment simulator (NJES) test assembly.

Hot-Fire Tests

Two series of short-duration, hot-fire tests using flight hardware were used to evaluate the redesigned case-to-nozzle joint under pressurized conditions. The nozzle joint environment simulator (NJES) shown in Fig. 6, was used in a series of tests performed at the test facility; the series consisted of five separate test runs. The transient pressure test article (TPTA), shown in Fig. 7, was used in a series of tests performed at the Marshall Space Flight Center (MSFC) where, again, the series consisted of five separate test runs. The test hardware for both series was designed so that the chamber pressure and the chamber pressure rise rate that occurs immediately after ignition duplicates that in the full-scale, full-duration motors. Flaws were deliberately placed in the joint bondline and through the wiper and primary O-rings to determine how the redesigned joint would function with a portion of the redundant sealing system disabled prior to motor operation. The dimensions of the adhesive bondline flaws were typical of those observed in the NJAD tests. The O-ring flaw dimensions were derived from observations of damaged O-rings during NJAD and from analysis to determine the worst case O-ring flaw.

The final phase of the qualification process of the redesigned case-to-nozzle joint was a series of five full-scale, full-duration static test motors. Two motors in this series, Qualification Motor 6 (QM-6) and Product Verification Motor 1 (PV-1), contained deliberate flaws in the case-to-nozzle joint. The QM-6 had a leak path through the adhesive, and PV-1 had a leak path through the adhesive and the wiper O-ring. One of the five static test motors, Demonstration Motor 9 (DM-9), developed a leak path through the adhesive to the wiper O-ring during the joint assembly. The effect of temperature on the motors was also evaluated by firing motors at both extremes of the firing temperature requirement (PMBT = 40° to 90°F).

The results of the case-to-nozzle portion of the NJES, TPTA, and full-scale static test motor series are listed in Tables 1 and 2. The flow/thermal analyses of the flaw types in each motor is discussed in the following section.

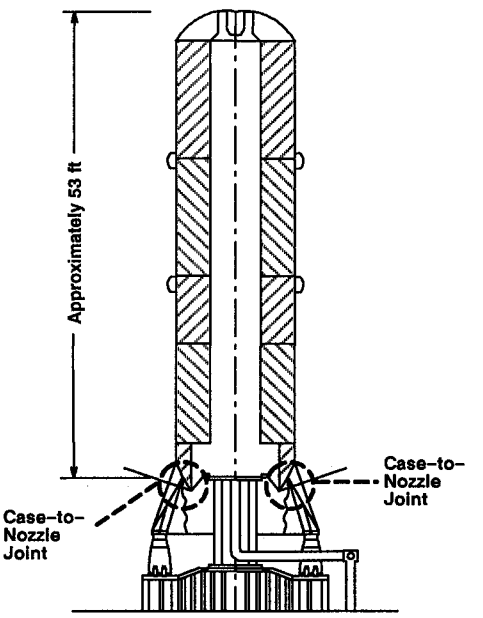

Fig. 7 Transient pressure test article (TPTA).

Table 1 Joint pressurization model comprehensive verification—nozzle joint

Model/flaw	NJES-1A, HPM[a]	NJES-2A, RSRM[b]	NJES-2B, RSRM[b]	NJES-3A, RSRM[b]	NJES-2B,RSRM[b]
Adhesive	0.35×0.16 in.	0.125×0.05 in.	0.125×0.05 in.	0.125×0.05 in.	0.125×0.05 in.
Wiper	NA	None	None	0.17×1.0 in.	0.17×1.0 in.
Primary	NA	None	None	None	0.17×1.0 inc.
ORING2	Good reconstructed pressure-time history; postpredicted 47 mils, erosion	Predict no erosion and no blowby	Predict no wiper erosion and no blowby	Predict 10 mils primary	Predict wiper burnthrough and 75 mils and no secondary erosion
PHOENICS Morton Thiokol '81) Nozzle joint	Measure temperature 293°F at 90°rt, 113°F at 90°lt, predicted temperature ambient 90 deg from flaw	NA	NA	NA	NA
Test results of flaw area	Pre-STS-51L design, no wiper in test, putty instead of adhesive, 45 mils erosion on primary	Adhesive flaw plugged at assembly; no wiper erosion	No erosion on wiper adhesive or insulation	No primary O-ring erosion with slight heat affect; max CP erosion: 5 mils; Max NBR erosion: 150 mils	Wiper burnthrough, 63 mil erosion on primary, no erosion on secondary; max CP erosion: 5 mils max NBR erosion: 150 mils

[a]High-pressure motor; used prior to STS-51L. [b]Redesigned solid rocket motor.

Table 2 Joint pressurization model comprehensive verification—nozzle joint

Model/flaw	TPTA 1.2, RSRM[a]	TPTA 1.3, RSRM[a]	TPTA 2.1, RSRM[a]	TPTA 2.2, RSRM[a]	PVM-1, RSRM-fullscale
Adhesive	0.125×0.05 in.	0.35×0.05 in.	0.125×0.05 in.	0.125×0.05 in.	0.125×0.05 in.
Wiper	0.17×1.0 in.	0.17×1.0 in.	0.17×1.0 in.	0.17×1.0 in.	0.17×1.0 in.
Primary	NA	None	None	None	0.17×1.0 in.
ORING2	Predict 12.8 mils primary erosion	Predict near wiper burnthrough, 36 mils primary and no secondary	Predict near wiper burnthrough and 13 mils primary erosion	Predict wiper burnthrough, 55 mils primary no secondary erosion	Predict wiper burnthrough, 14 mils primary and no secondary erosion
Test results of flaw area	Primary erosion 5 mils; max NBR erosion: 125 mils. max CP erosion: 30 mils; good agreement with measured $p(t)$-history	Wiper burnthrough, no primary or secondary erosion; no NBR or CP erosion; lack of erosion attributed to NBR structure inch-off aft of wiper and joint moisture	Wiper burnthrough no primary erosion; max NBR erosion: 50 mils; no CP erosion, poor agreement on pressure transient, possible NBR structure pinchoff	No erosion on any O-rings; no NBR or CP erosion; leak path blockage due to NBR structure pinch-off	Wiper burnthrough, primary erosion: 6 mils, no secondary erosion; slight NBR and CP erosion; poor $p(t)$ + history due to leak path plugging

[a]Redesigned solid rocket motor.

Flow/Thermal Overview

The major portion of the flow/thermal analyses relates to the case-to-nozzle joint pressurization and subsequent heating due to the entrance of chamber gases into the joint interior via postulated single- or double-leak paths through the joint bondline adhesive. The analyses conducted were those necessary to satisfy the agreed upon fail-safe and design/reuse criteria shown in Table 3. Along with the pertinent CEI specifications, these analyses represent the flow/thermal contribution to the critical design review (CDR) effort. The validity of the analyses is supported by the analysis verification plan, and the tests shown in Tables 1 and 2.[6]

Void volumes associated with pressurization analyses are shown in Fig. 8. They are defined as follows: V_3 is the volume (0.13 in.^{3}) of the polysulfide adhesive flaw in front of the wiper O-ring, V_1 is the volume (8.8 in.^{3}) behind the wiper O-ring in contact with insulation materials, V_2 is the volume (5.9 in.^{3}) of the primary O-ring cavity and is in contact with steel, and V_4 is the volume (17.26 in.^{3}) aft of the primary O-ring up to the secondary O-ring.

The design/reuse case (Fail-Safe/Design Category II) of Table 3 contains the most likely occurring single-leak path flaw. Analysis for this case only involves filling of the V_3 volume. The design/reuse criterion stipulates that the metal remain below the reusable local temperature (1080°F) and that no O-ring degradation occurs. Only one case, the single leak path to the wiper, is classified as a design/reuse situation. Since this flaw occurs the most often, it will be discussed later in more detail.

The fail-safe criterion (Fail-Safe/Design Category I) of Table 3 postulates the occurrence of at least one bondline adhesive flaw in line with at least one O-ring flaw. On a statistical basis, these conditions are considered to be very unlikely and are not a part of normal operation. Such a condition inevitably leads to O-ring degradation. However, the analyses show sufficient design margin to assure sealing capability and retain full operation for a safe continuation of the mission.[7] There are four single-leak path scenarios listed as follows: 1) large path to the primary O-ring, 2) large path to the secondary O-ring, 3) small path to the primary O-ring, and 4) small path to the secondary O-ring.

These four flaws were determined to be the most important from the viewpoint considering the likelihood of occurrence and severity. The analysis shows that the small path to the secondary O-ring was the most severe because of the long fill time. This case will be discussed later in more detail.

Double-leak path analyses have been performed for the following two flaw sizes in the joint polysulfide adhesive: 1) 0.125 by 0.050 in. and 2) 3.00 by 0.050 in.

The two cases are viewed as bounding the potential circumferential flow problem. The smaller adhesive flaw is of the approximate size of single-leak paths observed in full-scale tests to date. The smaller flaw produces higher impingement velocities but introduces less total energy into the joint. Maximum steel surface temperatures are comparable for both flaws and for both flaws the primary O-ring between 10 to 20 s into the motor operation. The presentation of the double-leak path results will concentrate on the smaller flaw.

O-ring Flaw Sizes

The single-leak path past the wiper has been examined for four different cases. Each of these cases was considered to be a fail-safe condition created by multiple flaws. The first two cases used a large flaw (1 by 0.10 in.) through the wiper O-ring, caused by joint assembly, and for the following postulated leak paths: 1) to the primary O-ring only and 2) past the primary to the secondary. The remaining two cases used the small contaminant wiper flaw (0.0887×0.0033 in.) that eroded with time for the following postulated leak paths: 1) to the primary O-ring only and 2) past the primary to the secondary.

Conservative leak path dimensions (0.125 by 0.050 in.) were chosen for the bondline adhesive based upon NJAD and NJES assembly data. The wiper O-ring flaw is based on observed data for O-rings cut during assembly. The contaminant flaw is considered to be an equivalent rectangular duct having approximately the same flow area and hydraulic diameter as a proposed triangular flaw (0.010 by 0.075 in.) void space enclosing a 0.010-in.-diam circular contaminant. This geometry describes the void space underneath an O-ring when the O-ring deforms around a wire-like contaminant.

A contaminant flaw in the primary O-ring was determined to be more severe than a large flaw. This is because the gas jet would have a direct path between radial bolts shown in Fig. 1 to the secondary O-ring. In contrast, the large primary O-ring flaw was determined to be less dangerous because the hot gas would have to flow around a radial bolt to reach the secondary O-ring. In addition, a smaller jet with a longer fill time would increase the total heating of the steel and Viton O-rings.

It should be noted that the postulated O-ring flaws used in the analyses are considerably larger than those that would be expected to be passed by the leak-check test criterion. The leak check is a specific test performed by pressurizing the volume between the primary and secondary O-ring through the leak check port. The leak check test flow rate is currently set at 0.1 sccs at 1000 psig. The postulated flaws used in the analyses exceed in severity the actual flaw sizes detectable after assembly.

Joint Pressurization Model

The general approach to the joint flaw analyses consisted first of a one-dimensional, lumped, parameter, volume-filling analysis followed by a more comprehensive three-dimensional, heat-conduction analysis using the SINDA computer code. The mass flow rates used in the SINDA calculations were predicted from a joint pressurization model (JPM), which included a simplified heat transfer model to solve the conjugate problem (coupled convection and conduction heat transfer). The ORING2 code, which was developed to calculate O-ring erosion also has the capability of predicting joint pressurization through a dual volume approach.[8]

For the detailed thermal analyses, the implicit solution scheme available in SINDA was implemented. The convective heat transfer coefficient was evaluated for each gas node adjacent to a solid surface. If the gas flow was determined to be turbulent, the Colburn equation was used.[9] For laminar gas flow ($Re \leq 2100$), a constant Nusselt (Nu) number was used, which was a function of the width and height of the gas node.[10] When the gas jet impinged on a surface, the jet-impingement heat transfer coefficient[11] was calculated.

As an independent effort, a three-dimensional calculation was performed for pressurizing volumes V_1, V_2, and V_3 through a single-leak path using the PHOENICS code.[12] At $T = 0.6$ s, the pressure at the flaw location was about 85% of the chamber pressure, whereas on the opposite side of the joint at the 180-deg location, the pressure was about 75% of that in the chamber. Flow velocities calculated by PHOENICS were comparable to those calculated by the one-dimensional, lumped parameter JPM. The 4400°F gas temperature calculated by PHOENICS at 0.6 s is comparable to the SINDA calculated 3789°F temperature at the location of the primary O-ring. As expected, the three-dimensional PHOENICS calculated gas temperatures are considerably lower at the 90-deg and 180-deg circumferential locations away from the joint flaw.

A summary of the JPM verification effort using the full-scale hardware is shown in Tables 1 and 2. All four single-leak path scenarios are represented along with the single adhesive flaw to the wiper O-ring only. The small flaw contaminant previously mentioned is not strictly represented because of the need to guarantee pressure-assuring flaws in the test hardware after assembly. In all the tests, the intentional flaws demonstrated less O-ring erosion than predicted. This discrepancy has been attributed to leak path plugging with soot and adhesive. In addition structural calculations have shown that the NBR material on the aft-segment side of the joint deforms into the gap ahead of the primary O-ring restricting the flow.[4]

Table 3 Fail-safe and design/reuse categories for nozzle joint flaws

Description		Condition	Category	Adhesive flaw	Wiper flaw	Primary flaw	V1	V2	V3	V4[a]
Single-leak path	Large path primary O-ring	Fail-safe	I	0.05×0.125 in.	0.1×1.0 in.	None	8.8	5.9	0.13	17.26
	Large path to secondary O-ring	Fail-safe	I	0.05×0.125 in.	0.1×1.0 in.	0.0033 in. × 0.00887 in.[b]	8.8	5.9	0.13	17.26
	Small path to primary O-ring	Fail-safe	I	0.25×0.125 in.	0.0033 in. × 0.00887 in.[b]	None	8.8	5.9	0.13	17.26
	Small path to secondary O-ring	Fail-safe	I	0.05×0.125 in.	0.0033 in. × 0.00887 in.[b]	0.0033 in. × 0.00887 in.[b]	8.8	5.9	0.13	17.26
	Path to wiper	Design	II	Unspecified	None	None	8.8	5.9	0.13	17.26
Double-leak path	Large flaw	Fail-safe	I	0.05×3.0 in., two at 120 deg	0.1×1.0 in.	None	8.8	5.9	0.13	17.26
	Small flaw	Fail-safe	I	0.05×0.125 in., two at 120 deg	0.1×1.0 in.	None	8.8	5.9	0.13	17.26

[a]Volumes V1 through V4 are expressed in units of cubic inches.
[b]The rectangle flaw 0.0033 by 0.00887 in. is equivalent on a flow basis to the proposed triangular flaw with dimensions 0.01 by 0.075 in. enclosing a circular contamination 0.01 in. diam.

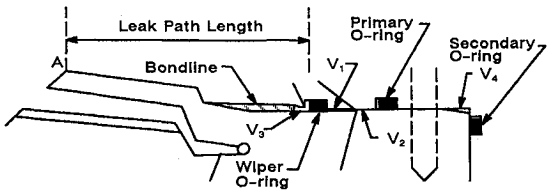

- Leak path length = 4.87 inches
- Leak path width and height in inches expressed as (width by height)
- Volumes
  V_1 = 8.8 in^3 V_3 = 0.13 in^3
  V_2 = 5.9 in^3 V_4 = 17.26 in^3
- Pressure differential due to nozzle vectoring will exist between entrance (A) to leak paths at different circumferential locations (double leak path scenario)

Fig. 8 Case-to-nozzle joint definitions for flow/thermal analyses (view in axial plane).

- ORING2 Model
- Leak path dimensions (initial):
  H = 0.050 in. W = 0.125 in. (adhesive)
  H = 0.0033 in. W = 0.0887 in. (wiper)
  H = 0.0033 in. W = 0.0887 in. (primary)
- Ablation, jet spreading, path erosion
- Variable flow path length
- Volumes: V_1 = 8.80 in.^{3} V_3 = 0.13 in.^{3}
  V_2 = 5.90 in.^{3} V_4 = 17.26 in.^{3}
- MF = 0.05

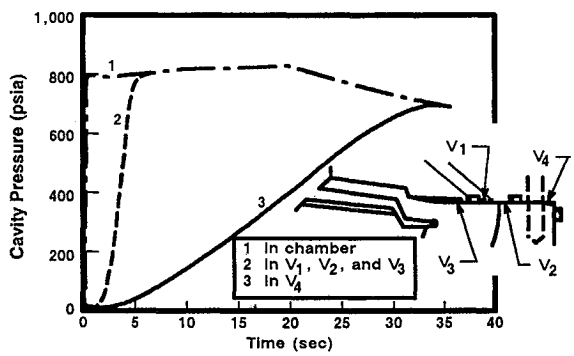

Fig. 9 Pressures in bonded case-to-nozzle joint due to a single leak path pressurization of volumes V_1, V_2, V_3, and V_4.

Single-Leak Path to the Wiper O-ring

The single-leak path through polysulfide adhesive leading to and not past the wiper O-ring is uneventful. This is because the small fill-volume V_3 is pressurized by a relatively large cross-sectional flow area. In such cases, the fill-volume pressurizes instantly and has the same transient as the motor pressure. As a result no appreciable jet impingement and no O-ring degradation occurs. This fact was confirmed by the QM-6[13] full-scale static test and the NJES-2B[14] subscale test. In both cases, hot chamber gas penetrated the defect in the adhesive to the forward edge of the wiper O-ring. The polysulfide adhesive surrounding the defect was heat affected up to 0.50 in. into the bondline. No erosion or heat effect was noted on the wiper O-ring. No rise in pressure was observed aft of the wiper O-ring. This shows that even though the wiper O-ring was not designed to seal off chamber pressure, it is capable of doing so if the polysulfide adhesive contains a leak path.

The largest available V_3 fill-volume recorded was in the DM-9 static test motor. It was calculated to be 17.5% of the unfilled wiper O-ring cavity. Using ORING2 with the measured bondline flaw dimensions of 0.2 by 0.05 in. and a joint pinching motor pressure of 230 psi, the observed DM-9

- ORING2 Model
- Leak path dimensions (initial):
  H = 0.050 in. W = 0.125 in. (adhesive)
  H = 0.0033 in. W = 0.0887 in. (wiper)
  H = 0.0033 in. W = 0.0887 in. (primary)
- Ablation, jet spreading, path erosion
- Variable flow path length
- Volumes: V_1 = 8.80 in.^{3} V_3 = 0.13 in.^{3}
  V_2 = 5.90 in.^{3} V_4 = 17.26 in.^{3}
- MF = 0.05
- 3D SINDA calculations

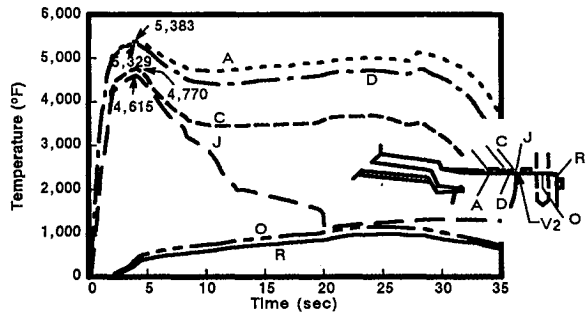

Fig. 10 Gas temperatures in bonded case-to-nozzle joint due to a single leak path pressurization of volumes V_1, V_2, and V_3 then pressurization of volume V_4.

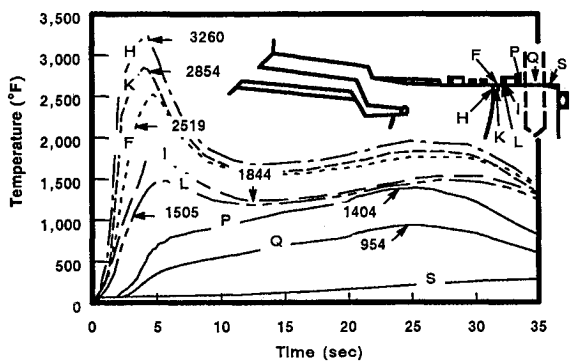

- ORING 2 Model
- Leak path dimensions (initial):
  H = 0.050 in. W = 0.125 in. (adhesive)
  H = 0.0033 in. W = 0.0887 in. (wiper)
  H = 0.0033 in. W = 0.0887 in. (primary)
- Ablation, jet spreading, path erosion
- Variable flow path length
- Volumes: V_1 = 8.80 in.^{3} V_3 = 0.13 in.^{3}
  V_2 = 5.90 in.^{3} V_4 = 17.26 in.^{3}
- MF = 0.05
- 3D SINDA calculations

Fig. 11 Steel temperature in bonded case-to-nozzle joint due to a single leak path pressurization of volumes V_1, V_2, V_3 then pressurization of volume V_4.

results of no wiper O-ring erosion were matched.[15] This calculation shows compliance with CEI specification in that manufacturing geometry deviations do not significantly affect wiper O-ring performance for a flaw only to and not past the wiper. The joint pinching pressure is based on the structural considerations that show NBR material on the relief flap side deforming into the adhesive bondline. This restricts the flow path leading to the wiper O-ring.

Single-Leak Path Through Small Wiper Opening to Secondary

Shown in Figs. 9–11 are the results of pressurizing volumes V_1, V_2, V_3, and V_4 via contaminant size flaws through both

Table 4 Bonded nozzle-case-joint circumferential flow studies

Cause	Circumferential Flow		Joint Response	
	Analysis	Test	Analysis	Test
Nozzle vectoring	1) Morton Thiokol PHOENICS	1) ARC water tunnel	1) Morton Thiokol 1D flow 3D SINDA	1) Morton Thiokol cold flow test
	2) Flow science FLOW-3D	2) NASA (MSFC)/SRS Technologies	2) NASA (MSFC)/Teledyne Brown SINDA/SINFLO	2) NASA (MSFC)/Coleman 2D cold flow test
	3) Creare FLUENT		3) Creare/Wickmann FLUENT, CMA	3) Morton Thiokol FHPC motor test
	4) NASA (MSFC)/CFD Research Corp PHOENICS		4) NASA (MSFC)/CFD Research PHOENICS	
	5) NASA (MSFC)/ Continuum, Inc. CONTINUSYS			
	6) NASA (MSFC)/ Lockheed PAID			

the wiper and primary O-rings. By definition, V_4 is the volume between the primary and secondary O-rings and includes the volume between two adjacent radial bolts. Of this volume, approximately 17% is represented by the region downstream of the corner.

The ORING2 model being one-dimensional cannot determine the fraction of the total mass flow entering V_4, which will impinge upon the secondary O-ring. This mass fraction (MF) was determined from a PHOENICS 81 calculation in which the region between the primary and secondary O-rings was modeled. In this calculation, the time-dependent boundary conditions $[P(t), T(t)]$ at the primary O-ring flaw were those calculated by ORING2.

The PHOENICS calculation involved solving the compressible, transient, Navier-Stokes equations using the κ-ϵ turbulence model. The calculation being fully conjugate, i.e., fluid-solid heat transfer coupled, determines the steel and O-ring surface temperatures, the steel temperature distribution, and the gas jet spreading in volume V_4 as a function of time. The MF calculated by PHOENICS was MF = 0.0128, which compares with the conservative value MF = 0.05 chosen for ORING2. This MF along with the ORING2 calculated mass flow into volume V_4 was then used in the SINDA code to calculate the joint temperatures.

The metal gap region in front of the primary O-ring is predicted to exceed the melting temperature of steel (2760°F) for about 3 s. This temperature is localized and applies over a circumferential width of less than 0.25 in. Other studies also suggest that the temperature estimates may be conservative because of the coarse computational mesh used in the near-surface nodes of the SINDA model. The results show that although the joint will not comply with the design/reuse requirements, it will satisfy the fail-safe conditions. While these calculations were in progress, actual hardware measurements in the DM-9, case-to-nozzle joint indicated that volume V_1 was, in fact, 5.67 in.^{3} and not 8.80 in.^{3} This 36% decrease in volume would greatly reduce predicted joint temperatures.

The maximum nodal temperatures for pressurization of volumes V_1, V_2, V_3, and V_4 are summarized as follows: 1) maximum localized steel temperature is 3260°F, and 2) maximum surface temperature of secondary O-ring is 675°F.

Thermal stress analyses show that the brief excursion to elevated temperatures does not compromise the structural integrity of the joint. The predicted secondary O-ring surface temperature is less than the ablation temperature (805°F) and experiences no degradation. The conclusion is that the case-to-nozzle joint can tolerate a single leak through a small opening (0.0887 by 0.0033 in.) in both the wiper and the primary O-ring and sustain no degradation to the secondary O-ring.

Double-Leak Path Model

The double-leak path consists of two adhesive flaws in line with two wiper O-ring defects that are connected to each other by the primary O-ring groove. After the initial pressurization, flow is induced in the path by the circumferential pressure gradient imposed by nozzle vectoring during motor operation. A survey of the analyses and tests[16] that were performed to evaluate circumferential flow and joint response is shown in Table 4.

In the analytical model, circumferential flow in the case-to-nozzle joint is assessed using externally coupled one-dimensional flow and three-dimensional heat transfer models. The one-dimensional fluid flow model solved for the steady-state, incompressible, gas-mass, flow rate through a network in which pressure at both ends of the network was specified using the Modified Lenkel Method (MLM).[17] The network considered reflects the dual insulation defect scenario: a single-passage entrance is followed by a 90-deg turn, division into multiple parallel flow passages (the free volume), a second 90-deg turn, and a single-passage exit. Flow rates determined were used to drive a SINDA heat transfer model. Assumed gas temperatures in the flow model were revised if necessary using SINDA results. Final flow rates and temperatures were used to predict O-ring erosion.

The analysis used in assessing circumferential flow effects contains substantial simplifications. The twin flaws are always considered to be aligned with the maximum circumferential pressure differential, irrespective of the plane of nozzle vectoring. Positive vectoring was considered to have the same effect as negative vectoring and did not reverse the direction of flow within the joint. The coarse one-dimensional flow network was used in estimating mass flow into the joint neglects flow resistance between the wiper and primary O-rings and other minor losses. The result of these simplifications was expected to be an overestimate of gas flow into the joint.

Combustion gas thermodynamic and transport properties used in the analyses include contributions of a condensed aluminum oxide phase. Full-scale tests in which intentional flaws were cut into the case-to-nozzle joint show that such slag is effectively separated from the gas by impingement on the step-like jog in the entrance leak path, upstream of the wiper O-ring. The present modeling makes no provision for this phenomenon; hence, energy convection downstream of the jog is expected to be overestimated.

Comparison to Cold Flow Test

A comparison has been made between the network predictions using the one-dimensional joint flow model and results

from the circumferential cold flow tests.[17] Predicted velocities are somewhat below measured values, but are in reasonable agreement. Because of the small differential pressures involved in the test and the accompanying uncertainties, strict comparisons are inconclusive.

Comparison to 400-lb Charge Motor Test Results

The 400-lb charge (FHPC) motor test was devised to investigate the problem of double-leak, path O-ring erosion, the relief flap and baffle erosion, and the concept of vented joints. The test consists of an FHPC motor in tandem with a test fixture simulating the case-to-nozzle joint. The hot exhaust gas travels the length of the center port or bore in the test fixture and finally exits through a nozzle insert that chokes the flow. The velocities generated in the test section were high on the order of $M=0.11$ and represented a worst-case environment for relief flap and baffle erosion. In contrast, the boundary condition or differential pressure established in the bore of the test section appeared inadequate to induce flow in the double-leak path. In all the FHPC motor tests, only slight or no O-ring erosion has been observed. Many technical explanations have been advanced for this discrepancy. The most likely reason has been provided by an analytical reassessment of the design of the FHPC test.[18] The FHPC motor test relies on a frictional pressure drop down the bore to establish the differential pressure to induce the double-leak, path-flow phenomena. As a consequence, not enough total pressure remained available to overcome the flow resistance of the double-leak path. This discredited any comparison of the FHPC test results and the thermal predictions for the RSRM nozzle joint. Further work to correct the problem was discontinued because the chance of a circumferential flow path occurring was assessed as being very unlikely.[19] To have circumferential flow in the case-to-nozzle joint, the following must occur: at least two polysulfide blowholes must align with at least two wiper O-ring defects, the two aligned leak paths must be separated by a certain distance, and the leak paths must align in the predominant plane of nozzle vectoring.

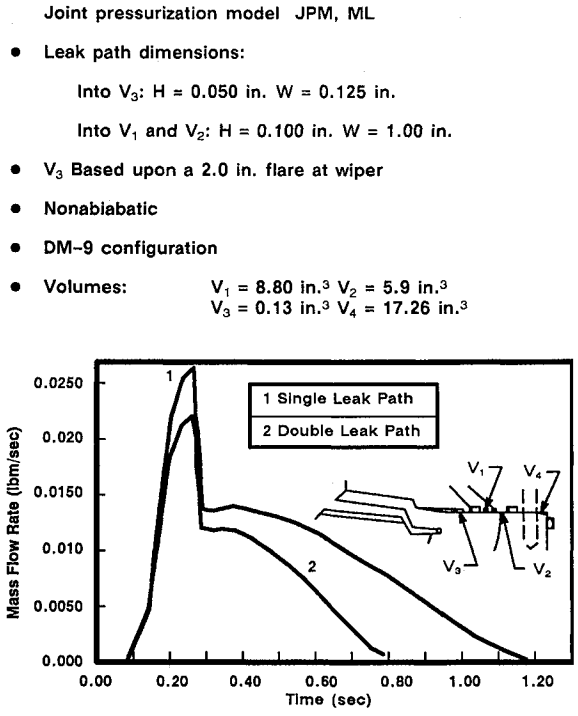

Fig. 12 Flow rates in bonded case-to-nozzle joint due to a single- and double-leak path filling of volumes V_3, V_1, and V_2.

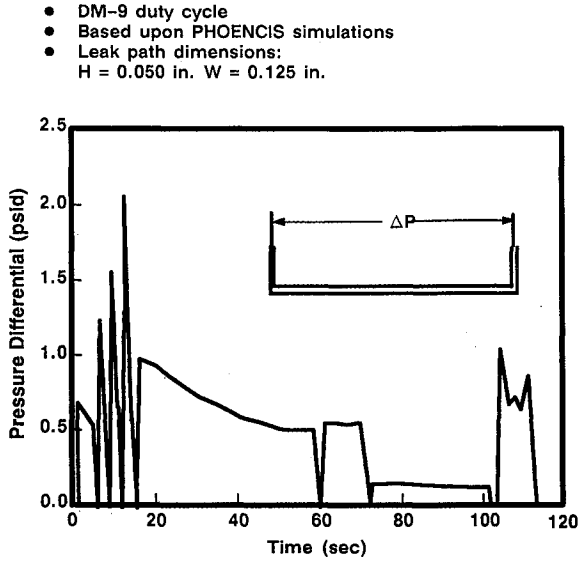

Fig. 13 Pressure difference between double-leak paths.

Double Leak with 0.125- by 0.050-in. Flaw

Shown in Fig. 12 is the mass flow rate for pressurization. The gas temperature reaches a maximum of 5300°F in the joint and decreases to about 4000°F during circumferential flow. Steel surface temperatures were predicted to exceed the melting point during pressurization, which indicates local hardware damage.

Following joint pressurization, circumferential flow is established in the double-leak path. Shown in Fig. 13 is the predicted maximum circumferential pressure difference calculated by PHOENICS for the internal motor flowfield using the DM-9 nozzle-vector duty cycle. Qualitatively, the mass flow rates along the primary O-ring followed the pressure differential and had a magnitude of approximately 0.006 lbm/s. The flow rates computed in the MLM network model were combined with the pressurization flow rates and used as input to a three-dimensional SINDA model of the joint interior.

The surface temperature decreases rapidly after pressurization but continued to exceed the reuse temperature throughout much of the period of circumferential flow as shown in Fig. 14. The gas temperature qualitatively follows the mass flow

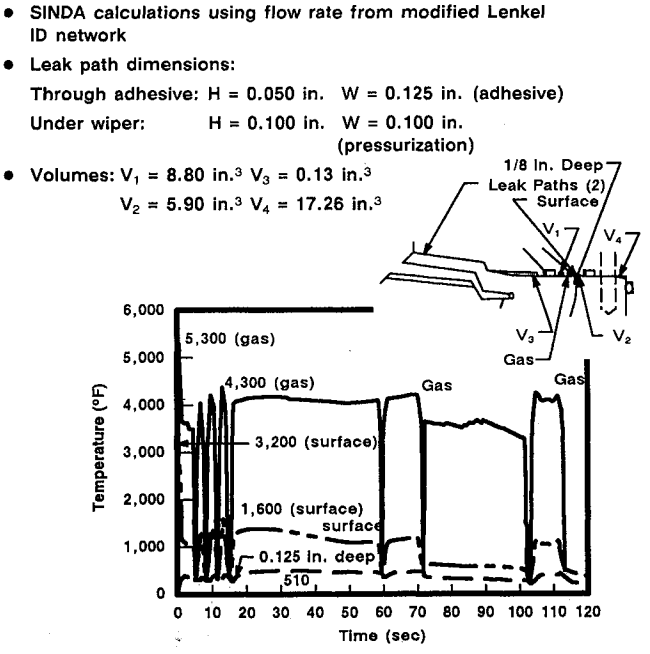

Fig. 14 Gas and steel temperatures in bonded case-to-nozzle joint due to circumferential flow from nozzle vectoring.

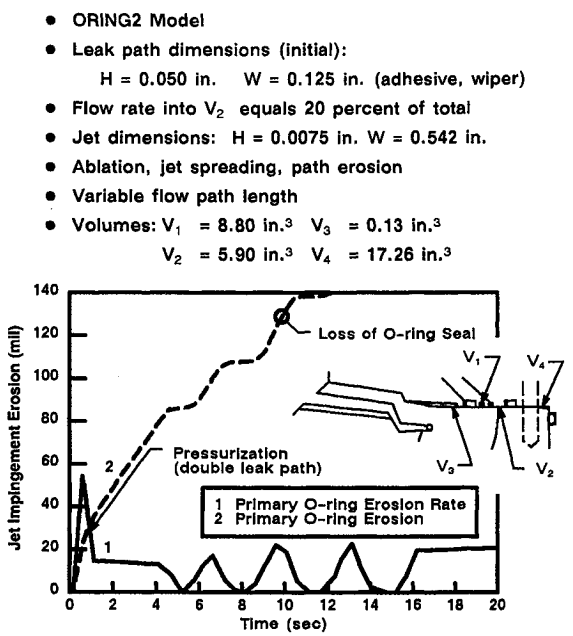

Fig. 15 Primary O-ring erosion in bonded case-to-nozzle joint due to a single-leak path pressurization of volumes V_1, V_2, V_3, and circumferential flow.

rate. The high surface temperatures do not penetrate far into the hardware. The hottest in-depth steel node, 0.125 in. from the exposed surface, remained below approximately 500°F throughout the entire firing. Heat effects in the primary O-ring were limited to a distance of about 1 in. on either side of the entrance leak path. The general severity of the double-leak path was confirmed by other independent analyses.[16]

The high gas temperatures led to predictions of primary O-ring failure within about 10 s after motor ignition. Shown in Fig. 15 is the predicted erosion rate (curve 1) and erosion (curve 2) for the primary O-ring as calculated by ORING2 during pressurization and circumferential flow. This impingement erosion was calculated in the same manner as the single-leak path erosion. Primary O-ring erosion of 0.133 in. was predicted at the end of 10 s. Since this amount of erosion equals the O-ring footprint, it means failure of the primary O-ring. As a result, the eroded O-ring provides a natural means for volume V_4 to pressurize without having to assume a flow path through the primary O-ring. An analysis using ORING2 was done to investigate the effects of pressurization on the secondary O-ring. The gas temperature has been shown to decrease after passing through the insulation leak path, through the metal-to-metal gap forward of the primary, and the smaller metal-to-metal gap behind the primary. This latter gap was assumed to be 0.00275 in. at full motor pressurization. Because of the small gap height and the high thermal conductivity of steel, the gas cools to below the 805°F ablation temperature of the Viton secondary O-ring. The result is no erosion of the secondary O-ring, although heat effect may be present. Similar results have been obtained for the larger 3-in. flow.

The predicted localized steel temperature exceeds the 1080°F limit for steel reuse during the volume-filling processes; however, thermal stress analyses showed that the brief excursion to elevated temperatures does not compromise the structural integrity of the joint.

Conclusion

The most important conclusions are listed as follows.

1) Major improvements to the case-to-nozzle joint include the incorporation of an unvented bonded joint, the addition of a pressure-actuated flap gap next to the bondline, the addition of an adhesive wiping O-ring, and the addition of 100 bolts in the radial direction to restrict joint movement.

2) The polysulfide adhesive flaw to and not past the wiper O-ring is uneventful and complies with all the applicable CEI specification requirements This case is classified in the design/reuse category. All other cases analyzed have been classified in the fail-safe category.

3) Analyses have shown that with leaks in the adhesive bond line, the design will meet performance requirements throughout the period of motor operation even under worst-case conditions. These conditions were worst-case dimension tolerances for V_1, V_2, V_3, and V_4 volumes, worst joint-flaw dimensions, and metal part gaps.

4) Higher local temperatures are predicted for the small contaminant flaw (0.0887 by 0.0033 in.) than for the large opening (1.0 by 0.10 in.). However, this contaminant flaw size was considerably larger than the actual flaw defect size permitted by the allowable 0.1 sccs leak check test flow rate at 1000 psig.

5) The double-leak path through the wiper O-ring leads to a predicted primary O-ring burnthrough between 10 and 20 s after motor ignition. Calculations show no secondary O-ring erosion or degradation. It should be noted that the in-line flaw alignment for the double-leak path scenario is very unlikely.[19]

References

[1]Adams, F., "Prime Equipment Contract End Item Detail Specification," Morton Thiokol Space Operations, Brigham City, UT, CPW1-3600A, Oct. 1988.

[2]Hicken, S., "RSRM Internal Insulation Design Summary," Morton Thiokol Space Operations, Brigham City, UT, TWR-18133, Sept. 1988.

[3]Boraas, S. O., "Flow/Thermal/Erosion Predictions for the DM-8 Motor," Morton Thiokol Space Division, Brigham City, UT, TWR-16165, Aug. 1987.

[4]LaMont, D., "Nozzle Joint Insulation Structural Analysis," Morton Thiokol Space Operations, Brigham City, UT, TWR-17037, Apr. 1988.

[5]Cook, J., "Nozzle Joint Assembly Demonstration (NJAD), Final Report," Morton Thiokol Space Operation, Brigham City, UT, TWR-16628, Aug. 1987.

[6]Morstadt, R. A., "Aero/Thermal Analysis Verification Results (ANV-23)," Morton Thiokol Space Division, Brigham City, UT, TWR-17113 Rev A, Mar. 1988.

[7]Allred, L. D., "Definition and Application of Fail-Safe Criteria in RSRM Joints," Morton Thiokol Space Division, Brigham City, UT, TWR-18263, Rev A, June 1988.

[8]O'Malley, M., "A Model for Predicting RSRM Joint Volume Pressurization, Temperature Transients, and Ablation," AIAA Paper 88-3332, July 1988.

[9]Bennet, C. O., and Myers, J. E., "Momentum, Heat, and Mass Transfer," McGraw-Hill, New York, 1974, p. 376.

[10]Incropera, F. P., and DeWitt, D. P., "Fundamentals of Heat Transfer," Wiley, New York, 1981, p. 411.

[11]Shadlesky, P. S., "Stagnation Point Heat Transfer for Jet Impingement to a Plane Surface," *AIAA Journal*, Vol. 21, No. 8, Nov. 1982, pp. 1214–1215.

[12]Malone, M. B., "Nozzle/Case Joint, Single Maximum Defect Size Leak Path, 3-D Pressurization," Morton Thiokol Space Division, TWR-16990, Sept. 1987.

[13]Magnum, K., "Space Shuttle Qualification Motor No. 6 (QM-6)," Morton Thiokol Space Operations, Brigham City, UT, TWR-17372, June 1988.

[14]Ricks, G. A., "Nozzle Joint Environment Simulator 2B (NJES-2B) Final Test Report," Morton Thiokol Space Operations, Brigham City, UT, TWR-17011, Nov. 1987.

[15]O'Malley, M., "Flow Thermal and Erosion Predictions for QM-6," Morton Thiokol Space Operations, Brigham City, UT, Morton Thiokol L213-FY88-M153, Feb. 1988.

[16]"Redesigned Solid Rocket Motor Circumferential Flow Technical Interchange Meeting Final Report," Morton Thiokol Space Operations, Brigham City, UT, TWR-17788, Feb. 1988.

[17]Koehler, L., "Comparison of J-Seal Cold Flow Test Flow Velocities with Modified Lenkel Method Predictions," Morton Thiokol Space Division, Brigham City, UT, TWR-17531, Nov. 1987.

[18]Boraas, S. O., "Existence of Circumferential Flow in the RSRM Joints, Morton Thiokol Space Division, Brigham City, UT, TWR-18048, Feb. 1988.

[19]Allred, L. D., and Allen, A. R., "RSRM Nozzle/Case Joint Circumferential Flow Probability Analysis," Morton Thiokol Space Division, Brigham City, UT, TWR-18204, April 1988.